

Z Boson Pair Production in e^+e^- Collisions at $\sqrt{s}=183$ and 189 GeV

The OPAL Collaboration

Abstract

A study of Z boson pair production in e^+e^- annihilation at center-of-mass energies near 183 GeV and 189 GeV is reported. Final states containing only leptons, ($\ell^+\ell^-\ell^+\ell^-$ and $\ell^+\ell^-\nu\bar{\nu}$), quark and lepton pairs, ($q\bar{q}\ell^+\ell^-$, $q\bar{q}\nu\bar{\nu}$) and the all-hadronic final state ($q\bar{q}q\bar{q}$) are considered. In all states with at least one Z boson decaying hadronically, $q\bar{q}$ and $b\bar{b}$ final states are considered separately using lifetime and event-shape tags, thereby improving the cross-section measurement. At $\sqrt{s} = 189$ GeV the Z-pair cross section was measured to be $0.80^{+0.14}_{-0.13}(\text{stat.})^{+0.06}_{-0.05}(\text{syst.})$ pb, consistent with the Standard Model prediction. At $\sqrt{s} = 183$ GeV the 95% C.L. upper limit is 0.55 pb. Limits on anomalous $ZZ\gamma$ and ZZZ couplings are derived.

Submitted to Phys. Lett. B

The OPAL Collaboration

G. Abbiendi², K. Ackerstaff⁸, P.F. Akesson³, G. Alexander²², J. Allison¹⁶, K.J. Anderson⁹, S. Arcelli¹⁷,
 S. Asai²³, S.F. Ashby¹, D. Axen²⁷, G. Azuelos^{18,a}, I. Bailey²⁶, A.H. Ball⁸, E. Barberio⁸, R.J. Barlow¹⁶,
 J.R. Batley⁵, S. Baumann³, T. Behnke²⁵, K.W. Bell²⁰, G. Bella²², A. Bellerive⁹, S. Bentvelsen⁸,
 S. Bethke^{14,i}, O. Biebel^{14,i}, A. Biguzzi⁵, I.J. Bloodworth¹, P. Bock¹¹, J. Böhme^{14,h}, O. Boeriu¹⁰,
 D. Bonacorsi², M. Boutemur³¹, S. Braibant⁸, P. Bright-Thomas¹, L. Brigliadori², R.M. Brown²⁰,
 H.J. Burckhart⁸, J. Cammin³, P. Capiluppi², R.K. Carnegie⁶, A.A. Carter¹³, J.R. Carter⁵,
 C.Y. Chang¹⁷, D.G. Charlton^{1,b}, D. Chrisman⁴, C. Ciocca², P.E.L. Clarke¹⁵, E. Clay¹⁵, I. Cohen²²,
 O.C. Cooke⁸, J. Couchman¹⁵, C. Couyoumtzelis¹³, R.L. Coxe⁹, M. Cuffiani², S. Dado²¹,
 G.M. Dallavalle², S. Dallison¹⁶, R. Davis²⁸, A. de Roeck⁸, P. Dervan¹⁵, K. Desch²⁵, B. Dienes^{30,h},
 M.S. Dixit⁷, M. Donkers⁶, J. Dubbert³¹, E. Duchovni²⁴, G. Duckeck³¹, I.P. Duerdoth¹⁶,
 P.G. Estabrooks⁶, E. Etzion²², F. Fabbri², A. Fanfani², M. Fanti², A.A. Faust²⁸, L. Feld¹⁰, P. Ferrari¹²,
 F. Fiedler²⁵, M. Fierro², I. Fleck¹⁰, A. Frey⁸, A. Fürtjes⁸, D.I. Futyan¹⁶, P. Gagnon¹², J.W. Gary⁴,
 G. Gaycken²⁵, C. Geich-Gimbel³, G. Giacomelli², P. Giacomelli², D.M. Gingrich^{28,a}, D. Glenzinski⁹,
 J. Goldberg²¹, W. Gorn⁴, C. Grandi², K. Graham²⁶, E. Gross²⁴, J. Grunhaus²², M. Gruwé²⁵,
 P.O. Günther³, C. Hajdu²⁹, G.G. Hanson¹², M. Hansroul⁸, M. Hapke¹³, K. Harder²⁵, A. Harel²¹,
 C.K. Hargrove⁷, M. Harin-Dirac⁴, A. Hauke³, M. Hauschild⁸, C.M. Hawkes¹, R. Hawkings²⁵,
 R.J. Hemingway⁶, C. Hensel²⁵, G. Herten¹⁰, R.D. Heuer²⁵, M.D. Hildreth⁸, J.C. Hill⁵, P.R. Hobson²⁵,
 A. Hocker⁹, K. Hoffman⁸, R.J. Homer¹, A.K. Honma⁸, D. Horváth^{29,c}, K.R. Hossain²⁸, R. Howard²⁷,
 P. Hüntemeyer²⁵, P. Igo-Kemenes¹¹, D.C. Imrie²⁵, K. Ishii²³, F.R. Jacob²⁰, A. Jawahery¹⁷,
 H. Jeremie¹⁸, M. Jimack¹, C.R. Jones⁵, P. Jovanovic¹, T.R. Junk⁶, N. Kanaya²³, J. Kanzaki²³,
 G. Karapetian¹⁸, D. Karlen⁶, V. Kartvelishvili¹⁶, K. Kawagoe²³, T. Kawamoto²³, P.I. Kayal²⁸,
 R.K. Keeler²⁶, R.G. Kellogg¹⁷, B.W. Kennedy²⁰, D.H. Kim¹⁹, K. Klein¹¹, A. Klier²⁴, T. Kobayashi²³,
 M. Kobel³, T.P. Kokott³, M. Kolrep¹⁰, S. Komamiya²³, R.V. Kowalewski²⁶, T. Kress⁴, P. Krieger⁶,
 J. von Krogh¹¹, T. Kuhl³, M. Kupper²⁴, P. Kyberd¹³, G.D. Lafferty¹⁶, H. Landsman²¹, D. Lanske¹⁴,
 I. Lawson²⁶, J.G. Layter⁴, A. Leins³¹, D. Lellouch²⁴, J. Letts¹², L. Levinson²⁴, R. Liebisch¹¹,
 J. Lillich¹⁰, B. List⁸, C. Littlewood⁵, A.W. Lloyd¹, S.L. Lloyd¹³, F.K. Loebinger¹⁶, G.D. Long²⁶,
 M.J. Losty⁷, J. Lu²⁷, J. Ludwig¹⁰, A. Macchiolo¹⁸, A. Macpherson²⁸, W. Mader³, M. Mannelli⁸,
 S. Marcellini², T.E. Marchant¹⁶, A.J. Martin¹³, J.P. Martin¹⁸, G. Martinez¹⁷, T. Mashimo²³,
 P. Mättig²⁴, W.J. McDonald²⁸, J. McKenna²⁷, T.J. McMahon¹, R.A. McPherson²⁶, F. Meijers⁸,
 P. Mendez-Lorenzo³¹, F.S. Merritt⁹, H. Mes⁷, I. Meyer⁵, A. Michelini², S. Mihara²³, G. Mikenberg²⁴,
 D.J. Miller¹⁵, W. Mohr¹⁰, A. Montanari², T. Mori²³, K. Nagai⁸, I. Nakamura²³, H.A. Neal^{12,f},
 R. Nisius⁸, S.W. O'Neale¹, F.G. Oakham⁷, F. Odorici², H.O. Ogren¹², A. Okpara¹¹, M.J. Oreglia⁹,
 S. Orito²³, G. Pásztor²⁹, J.R. Pater¹⁶, G.N. Patrick²⁰, J. Patt¹⁰, R. Perez-Ochoa⁸,
 P. Pfeifenschneider¹⁴, J.E. Pilcher⁹, J. Pinfold²⁸, D.E. Plane⁸, B. Poli², J. Polok⁸, M. Przybycień^{8,d},
 A. Quadt⁸, C. Rembser⁸, H. Rick⁸, S.A. Robins²¹, N. Rodning²⁸, J.M. Roney²⁶, S. Rosati³,
 K. Roscoe¹⁶, A.M. Rossi², Y. Rozen²¹, K. Runge¹⁰, O. Runolfsson⁸, D.R. Rust¹², K. Sachs¹⁰,
 T. Saeki²³, O. Sahr³¹, W.M. Sang²⁵, E.K.G. Sarkisyan²², C. Sbarra²⁶, A.D. Schaile³¹, O. Schaile³¹,
 P. Scharff-Hansen⁸, S. Schmitt¹¹, A. Schönig⁸, M. Schröder⁸, M. Schumacher²⁵, C. Schwick⁸,
 W.G. Scott²⁰, R. Seuster^{14,h}, T.G. Shears⁸, B.C. Shen⁴, C.H. Shepherd-Themistocleous⁵,
 P. Sherwood¹⁵, G.P. Siroli², A. Skuja¹⁷, A.M. Smith⁸, G.A. Snow¹⁷, R. Sobie²⁶,
 S. Söldner-Rembold^{10,e}, S. Spagnolo²⁰, M. Sproston²⁰, A. Stahl³, K. Stephens¹⁶, K. Stoll¹⁰, D. Strom¹⁹,
 R. Ströhmer³¹, B. Surrow⁸, S.D. Talbot¹, S. Tarem²¹, R.J. Taylor¹⁵, R. Teuscher⁹, M. Thiergen¹⁰,
 J. Thomas¹⁵, M.A. Thomson⁸, E. Torrence⁸, S. Towers⁶, T. Trefzger³¹, I. Trigger⁸, Z. Trócsányi^{30,g},
 E. Tsur²², M.F. Turner-Watson¹, I. Ueda²³, R. Van Kooten¹², P. Vannerem¹⁰, M. Verzocchi⁸, H. Voss³,
 D. Waller⁶, C.P. Ward⁵, D.R. Ward⁵, P.M. Watkins¹, A.T. Watson¹, N.K. Watson¹, P.S. Wells⁸,
 T. Wengler⁸, N. Wermes³, D. Wetterling¹¹, J.S. White⁶, G.W. Wilson¹⁶, J.A. Wilson¹, T.R. Wyatt¹⁶,
 S. Yamashita²³, V. Zacek¹⁸, D. Zer-Zion⁸

- ¹School of Physics and Astronomy, University of Birmingham, Birmingham B15 2TT, UK
- ²Dipartimento di Fisica dell' Università di Bologna and INFN, I-40126 Bologna, Italy
- ³Physikalisches Institut, Universität Bonn, D-53115 Bonn, Germany
- ⁴Department of Physics, University of California, Riverside CA 92521, USA
- ⁵Cavendish Laboratory, Cambridge CB3 0HE, UK
- ⁶Ottawa-Carleton Institute for Physics, Department of Physics, Carleton University, Ottawa, Ontario K1S 5B6, Canada
- ⁷Centre for Research in Particle Physics, Carleton University, Ottawa, Ontario K1S 5B6, Canada
- ⁸CERN, European Organisation for Particle Physics, CH-1211 Geneva 23, Switzerland
- ⁹Enrico Fermi Institute and Department of Physics, University of Chicago, Chicago IL 60637, USA
- ¹⁰Fakultät für Physik, Albert Ludwigs Universität, D-79104 Freiburg, Germany
- ¹¹Physikalisches Institut, Universität Heidelberg, D-69120 Heidelberg, Germany
- ¹²Indiana University, Department of Physics, Swain Hall West 117, Bloomington IN 47405, USA
- ¹³Queen Mary and Westfield College, University of London, London E1 4NS, UK
- ¹⁴Technische Hochschule Aachen, III Physikalisches Institut, Sommerfeldstrasse 26-28, D-52056 Aachen, Germany
- ¹⁵University College London, London WC1E 6BT, UK
- ¹⁶Department of Physics, Schuster Laboratory, The University, Manchester M13 9PL, UK
- ¹⁷Department of Physics, University of Maryland, College Park, MD 20742, USA
- ¹⁸Laboratoire de Physique Nucléaire, Université de Montréal, Montréal, Quebec H3C 3J7, Canada
- ¹⁹University of Oregon, Department of Physics, Eugene OR 97403, USA
- ²⁰CLRC Rutherford Appleton Laboratory, Chilton, Didcot, Oxfordshire OX11 0QX, UK
- ²¹Department of Physics, Technion-Israel Institute of Technology, Haifa 32000, Israel
- ²²Department of Physics and Astronomy, Tel Aviv University, Tel Aviv 69978, Israel
- ²³International Centre for Elementary Particle Physics and Department of Physics, University of Tokyo, Tokyo 113-0033, and Kobe University, Kobe 657-8501, Japan
- ²⁴Particle Physics Department, Weizmann Institute of Science, Rehovot 76100, Israel
- ²⁵Universität Hamburg/DESY, II Institut für Experimental Physik, Notkestrasse 85, D-22607 Hamburg, Germany
- ²⁶University of Victoria, Department of Physics, P O Box 3055, Victoria BC V8W 3P6, Canada
- ²⁷University of British Columbia, Department of Physics, Vancouver BC V6T 1Z1, Canada
- ²⁸University of Alberta, Department of Physics, Edmonton AB T6G 2J1, Canada
- ²⁹Research Institute for Particle and Nuclear Physics, H-1525 Budapest, P O Box 49, Hungary
- ³⁰Institute of Nuclear Research, H-4001 Debrecen, P O Box 51, Hungary
- ³¹Ludwigs-Maximilians-Universität München, Sektion Physik, Am Coulombwall 1, D-85748 Garching, Germany

^a and at TRIUMF, Vancouver, Canada V6T 2A3

^b and Royal Society University Research Fellow

^c and Institute of Nuclear Research, Debrecen, Hungary

^d and University of Mining and Metallurgy, Cracow

^e and Heisenberg Fellow

^f now at Yale University, Dept of Physics, New Haven, USA

^g and Department of Experimental Physics, Lajos Kossuth University, Debrecen, Hungary

^h and MPI München

ⁱ now at MPI für Physik, 80805 München.

1 Introduction

The study of the process $e^+e^- \rightarrow ZZ$ has recently become possible since LEP now operates at center-of-mass energies above the threshold for on-shell Z boson pair production. In the Standard Model, the process $e^+e^- \rightarrow ZZ$ occurs via the NC2 diagrams [1] shown in Figure 1. The Z-pair cross section depends on properties of the Z boson (m_Z , Γ_Z and the vector and axial vector coupling of the Z to electrons, g_V^e and g_A^e) that have been measured with great precision at the Z resonance [2]. The expected Z-pair cross section increases from about 0.25 pb at $\sqrt{s} = 183$ GeV to about 1.0 pb at $\sqrt{s} = 200$ GeV, but remains more than an order of magnitude smaller than W-pair production. In contrast to W-pair production, where tree level $WW\gamma$ and WWZ couplings are important, no ZZZ and $ZZ\gamma$ couplings are expected in the Standard Model. However, physics beyond the Standard Model could lead to effective couplings [3] which could then be observed as deviations in the measured Z-pair cross section from the Standard Model prediction. Such deviations have been proposed in the context of Higgs doublet models [4] and in low scale gravity theories [5]. In this paper we report on measurements of the NC2 Z-pair cross section, including the extrapolation to final states with one or both Z bosons off-shell. These measurements, along with the angular distribution of the observed events, are then used to extract limits on possible ZZZ and $ZZ\gamma$ couplings.

In Section 2 we describe the data sets used and the Monte Carlo simulation of signal and background. In Section 3 we describe the selection of the processes $ZZ \rightarrow \ell^+\ell^-\ell^+\ell^-$, $ZZ \rightarrow \ell^+\ell^-\nu\bar{\nu}$, $ZZ \rightarrow q\bar{q}\ell^+\ell^-$, $ZZ \rightarrow q\bar{q}\nu\bar{\nu}$, and $ZZ \rightarrow q\bar{q}q\bar{q}$, where $\ell^+\ell^-$ denotes a charged lepton pair of opposite charge and $q\bar{q}$ any of the five lightest quark-antiquark pairs. We also describe analyses of $ZZ \rightarrow b\bar{b}\ell^+\ell^-$, $ZZ \rightarrow b\bar{b}\nu\bar{\nu}$ and $ZZ \rightarrow q\bar{q}b\bar{b}$ which use b-tagging methods similar to those used in the OPAL Higgs search [6]. The use of b-tagging improves the separation of the Z-pair signal from background and allows us to check the $b\bar{b}$ content of our Z-pair sample for consistency with the Standard Model. The description of the individual selections is followed by a discussion of possible systematic errors (Section 3.6). In Section 4 the selected events are used to measure the Z-pair cross section. Then the cross section and angular distribution are compared with the Standard Model predictions and limits on anomalous neutral current triple gauge couplings are derived.

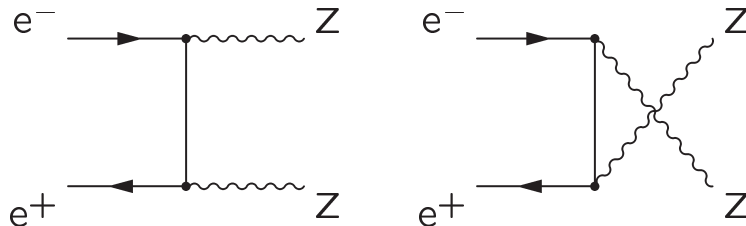


Figure 1: NC2 Feynman diagrams for the process $e^+e^- \rightarrow ZZ$ leading to a final state with four fermions.

2 Data analysis and Monte Carlo

The OPAL detector¹, trigger and data acquisition system are described fully elsewhere [7–11]. Our analyses use approximately 55 pb^{-1} of data collected at center-of-mass energies between 181–184 GeV and approximately 178 pb^{-1} collected at center-of-mass energies near 189 GeV. The corresponding luminosity-weighted mean center-of-mass energies are $182.62 \pm 0.05 \text{ GeV}$ and $188.63 \pm 0.04 \text{ GeV}$ [12]. The luminosity was measured using small-angle Bhabha scattering events recorded in the silicon-tungsten luminometer [11, 13, 14] and the theoretical calculation of Reference [15]. The overall error on the luminosity measurement amounts to less than 0.5% and contributes negligibly to our cross-section measurement error.

Selection efficiencies and backgrounds were calculated using Monte Carlo simulations. All events were passed through a simulation [16] of the OPAL detector and processed as for data. We define the ZZ cross section as the contribution to the total four-fermion cross section from the NC2 Z-pair diagrams shown in Figure 1. All signal efficiencies given in this paper are with respect to these Z-pair processes. Contributions from all other four-fermion final states, including interference with NC2 diagrams, are considered as background. For studies of the signal efficiency we have used `grc4f` [17], `YFSZZ` [18] and `PYTHIA` [19].

Backgrounds are simulated using several different generators. `PYTHIA` is used to simulate two-fermion final states such as $e^+e^- \rightarrow Z^*(n\gamma) \rightarrow q\bar{q}(n\gamma)$ and $e^+e^- \rightarrow \gamma^*(n\gamma) \rightarrow q\bar{q}(n\gamma)$, where $(n\gamma)$ indicates the generation of one or more initial state photons. `HERWIG` [20] and `KK2f` [21] are used as checks for these final states. These two-fermion generators include gluon radiation from the quarks which produce $q\bar{q}g$, $q\bar{q}q\bar{q}$ and $q\bar{q}gg$ final states. The `grc4f` generator, with the contribution exclusively due to NC2 diagrams removed, is used to simulate other four-fermion background. `KORALW` [22] and `EXCALIBUR` [23] are used as checks of the four-fermion background. Multiperipheral (“two-photon”) processes with hadronic final states are simulated by combining events from `PYTHIA`, for events without electrons scattered into the detector, and `HERWIG` [20], for events with electrons scattered into the detector. For the $q\bar{q}e^+e^-$ final state, `TWOGEN` [24] is used to simulate two-photon events with both the electron and positron scattered into the detector. The Vermaseren [25] generator is used to simulate multiperipheral production of the final states $e^+e^-\ell^+\ell^-$.

To avoid background from four-fermion final states mediated by $Z\gamma^*$, our selections were optimized to select simulated events with masses, m_1 and m_2 , that satisfy $m_1 + m_2 > 170 \text{ GeV}$ and $|m_1 - m_2| < 20 \text{ GeV}$. At 189 GeV (183 GeV) more than 90% (80%) of the events produced via the NC2 diagrams are contained in this mass region. Events from the NC2 diagrams dominate in this mass region except for final states containing electron pairs. Backgrounds in these samples from two-photon and electroweak Compton scattering ($e\gamma \rightarrow eZ$) processes [26] are reduced by using electrons detected in the electromagnetic calorimeters with $|\cos\theta_e| < 0.985$, where θ_e is the polar angle of the electron.

3 Event selection

In the following subsections we describe event selections which exploit every decay mode of the Z boson. Our selections cover all ZZ final states except $\nu\bar{\nu}\nu\bar{\nu}$ and $\tau^+\tau^-\nu\bar{\nu}$. In hadronic final states, the energy and direction of the jets are determined using reconstructed tracks and calorimeter clusters using the correction for double counting described in Reference [6]. In the $q\bar{q}\ell^+\ell^-$, $q\bar{q}q\bar{q}$ and $q\bar{q}b\bar{b}$ analyses four-constraint (4C) and five-constraint (5C) kinematic fits are used. The 4C fit imposes energy and momentum conservation. In the 5C fit the added constraint requires the masses of the two

¹OPAL uses a right-handed coordinate system in which the z axis is along the electron beam direction and the x axis is horizontal. The polar angle, θ , is measured with respect to the z axis and the azimuthal angle, ϕ , with respect to the x axis.

candidate Z bosons to be equal to one another. For final states with one or more Z bosons decaying to tau pairs, the energy and total momentum of the tau leptons are obtained by leaving the reconstructed direction of the four fermions fixed and scaling the energy and momentum of each of the fermions to obtain energy and momentum conservation. The scaled values of the tau momentum and energy are then used in the subsequent steps of the analysis. In the $q\bar{q}\tau^+\tau^-$ and $b\bar{b}\tau^+\tau^-$ final states, subsequent kinematic fits are effectively 2C and 3C fits.

3.1 Selection of $ZZ \rightarrow \ell^+\ell^-\ell^+\ell^-$ events

Z-pair events decaying to final states with four charged leptons ($\ell^+\ell^-\ell^+\ell^-$) produce low multiplicity events with a clear topological signature that is exploited to maximize the selection efficiency. The $\ell^+\ell^-\ell^+\ell^-$ analysis begins by selecting low multiplicity events (less than 13 tracks or clusters) with visible energy of at least $0.2\sqrt{s}$ and at least one track with momentum of 5 GeV or more. Using a cone algorithm, the events are required to have exactly four cones of 15° half angle containing between 1 and 3 tracks. Cones of opposite charge are paired² to form Z boson candidates.

Lepton identification is only used to classify events as background or to reduce the number of cone combinations considered by preventing the matching of identified electrons with identified muons. Electrons are identified on the basis of energy deposition in the electromagnetic calorimeter, track curvature and specific ionization in the tracking chambers. Muons are identified using the association between tracks and hits in the hadron calorimeter and muon chambers.

To reduce background from two-photon events with a single scattered electron detected, we eliminate events with forward going electrons (backward going positrons) with the cut $\cos\theta_{e^-} < 0.85$ ($\cos\theta_{e^+} > -0.85$). Here θ_{e^-} (θ_{e^+}) is the angle of the electron (positron) with respect to the incoming electron beam. Background from partially reconstructed $q\bar{q}(n\gamma)$ events and two-photon events is reduced by requiring that most of the energy is not concentrated in a single cone, $E_{\text{vis}} - E_{\text{cone}}^{\text{max}} > 0.2\sqrt{s}$. Here E_{vis} is the total visible energy of the event and $E_{\text{cone}}^{\text{max}}$ is the energy contained in the most energetic cone.

The invariant masses of the lepton pairs are calculated in three different ways which are motivated by the possibility of having zero, one or two tau pairs in the event. The events are classified according to the number of tau pairs in the event. (i) Events with $E_{\text{vis}} > 0.9\sqrt{s}$ are treated as $e^+e^-e^+e^-$, $e^+e^-\mu^+\mu^-$ or $\mu^+\mu^-\mu^+\mu^-$ events. We also treat all events with $|\cos\theta_{\text{miss}}| > 0.98$ (θ_{miss} is the polar angle associated with the missing momentum in the event) as $e^+e^-e^+e^-$, $e^+e^-\mu^+\mu^-$ or $\mu^+\mu^-\mu^+\mu^-$ events to maintain efficiency for Z-pairs with initial state radiation. In these events there are no missing neutrinos and the mass of each pair of lepton cones is evaluated. (ii) Events failing (i) with a cone-pair combination that has energy exceeding $0.9m_Z$ are tried as an $e^+e^-\tau^+\tau^-$ or $\mu^+\mu^-\tau^+\tau^-$ final state. The mass of the tau-pair system is calculated from the recoil mass of the presumed electron or muon pair. (iii) Any remaining combinations are treated as $\tau^+\tau^-\tau^+\tau^-$ final states. The momenta of the tau leptons are determined with the scaling procedure described in the introduction to Section 3 and the invariant masses of the cone pairs are evaluated using the scaled momenta. In any event with more than one valid combination, each combination is tested using the invariant mass cuts listed below.

To reduce the combinatorial background, combinations with pair masses closest to m_Z are selected. In events with one or more combination satisfying $|m_Z - m_{\ell\ell}| > 0.1m_Z$ the cone-pair combination with the smallest value of $(m_Z - m_{\ell\ell})^2 + (m_Z - m_{\ell'\ell'})^2$ is selected for further analysis. In the other combinations, the combination with the smallest value of $|m_Z - m_{\ell\ell}|$ or $|m_Z - m_{\ell'\ell'}|$ is selected. The final event sample is then chosen with the requirement $m_{\ell\ell} + m_{\ell'\ell'} > 160$ GeV and $|m_{\ell\ell} - m_{\ell'\ell'}| < 40$ GeV.

²Two-track cones are assigned the charge of the most energetic track if the momentum of one track exceeds that of the other by a factor of 4. Events with a cone which fails this requirement are rejected.

The signal detection efficiency, averaged over all $\ell^+\ell^-\ell^+\ell^-$ final states is given in Table 1 (line a). The efficiency for individual final states range from 30% for $\tau^+\tau^-\tau^+\tau^-$ to more than 70% for $\mu^+\mu^-\mu^+\mu^-$. The invariant masses of all cone pairs passing one of the selections are shown in Figure 2a. One candidate is found in the 183 GeV data and one candidate is found in the 189 GeV data.

3.2 Selection of $ZZ \rightarrow \ell^+\ell^-\nu\bar{\nu}$ events

The selection of the $e^+e^-\nu\bar{\nu}$ and $\mu^+\mu^-\nu\bar{\nu}$ final states is based on the OPAL selection of W pairs decaying to leptons [27]. The mass and momentum of the Z boson decaying to $\nu\bar{\nu}$ are calculated using the beam energy constraint and the visible decay of the other Z boson to a charged lepton pair. A likelihood selection based on the visible and recoil masses as well as the polar angle of the leptons, is then used to separate signal from background.

The $e^+e^-\nu\bar{\nu}$ selection starts with OPAL W-pair candidates where both charged leptons are classified as electrons. Each event is then divided into two hemispheres using the thrust axis. The highest momentum charged (leading) track is selected from each hemisphere. The sum of the charges of these two tracks is required to be zero. The determination of the visible mass, m_{vis} , and the recoil mass, m_{recoil} , is based on the energy as measured in the electromagnetic calorimeter and the direction of the leading tracks.

Three variables were chosen for the likelihood selection: $Q \cos \theta$, where θ is the angle of the highest momentum charged track and Q is its charge, the normalized sum of visible and recoil masses $(m_{\text{vis}} + m_{\text{recoil}})/\sqrt{s}$ and the difference of visible and recoil masses, $m_{\text{vis}} - m_{\text{recoil}}$. The performance of the likelihood is improved with the following preselection: $-25 \text{ GeV} < m_{\text{vis}} - m_{\text{recoil}} < 15 \text{ GeV}$ and $(m_{\text{vis}} + m_{\text{recoil}})/\sqrt{s} > 0.90$. One event with $\mathcal{L}_{e^+e^-\nu\bar{\nu}} > 0.60$ is selected (see Table 1 (line b) and Figure 3a).

The $\mu^+\mu^-\nu\bar{\nu}$ selection starts with the OPAL W-pair candidates where both charged leptons are classified as muons. The selection procedure is the same as for the $e^+e^-\nu\bar{\nu}$ final states except that m_{vis} , m_{recoil} , and E_{vis} are calculated from the the momentum of the reconstructed tracks of the Z boson decaying to muon pairs. The likelihood preselections $-25 \text{ GeV} < m_{\text{vis}} - m_{\text{recoil}} < 25 \text{ GeV}$ and $(m_{\text{vis}} + m_{\text{recoil}})/\sqrt{s} > 0.90$ are applied. Two events with $\mathcal{L}_{\mu^+\mu^-\nu\bar{\nu}} > 0.60$ are selected (see Table 1 (line c) and Figure 3b).

3.3 Selection of $ZZ \rightarrow q\bar{q}\ell^+\ell^-$ events

The lepton pairs in the $q\bar{q}e^+e^-$ and $q\bar{q}\mu^+\mu^-$ final states have a distinctive signature making possible selections with high efficiencies and a low background contamination. In the $q\bar{q}\tau^+\tau^-$ final state, the decay of the tau leptons produces events which are more difficult to identify. The identification of this final state exploits the missing momentum and missing energy carried away by the neutrinos produced in the decay of the tau lepton.

3.3.1 Selection of $ZZ \rightarrow q\bar{q}e^+e^-$ and $ZZ \rightarrow q\bar{q}\mu^+\mu^-$ events

The selection of $q\bar{q}e^+e^-$ and $q\bar{q}\mu^+\mu^-$ final states requires the visible energy of the events to be greater than 90 GeV and at least six reconstructed tracks. Among all tracks with momenta greater than 2 GeV, the highest momentum track is taken as the first lepton candidate and the second-highest momentum track with a charge opposite to the first candidate is taken as the second lepton candidate. Using the Durham [28] jet algorithm, the event, including the lepton candidates, is forced into four jets and the jet resolution variable that separates the three-jet topology from the four-jet topology, y_{34} , is required to be greater than 10^{-3} . Excluding the electron or muon candidates and their associated calorimeter

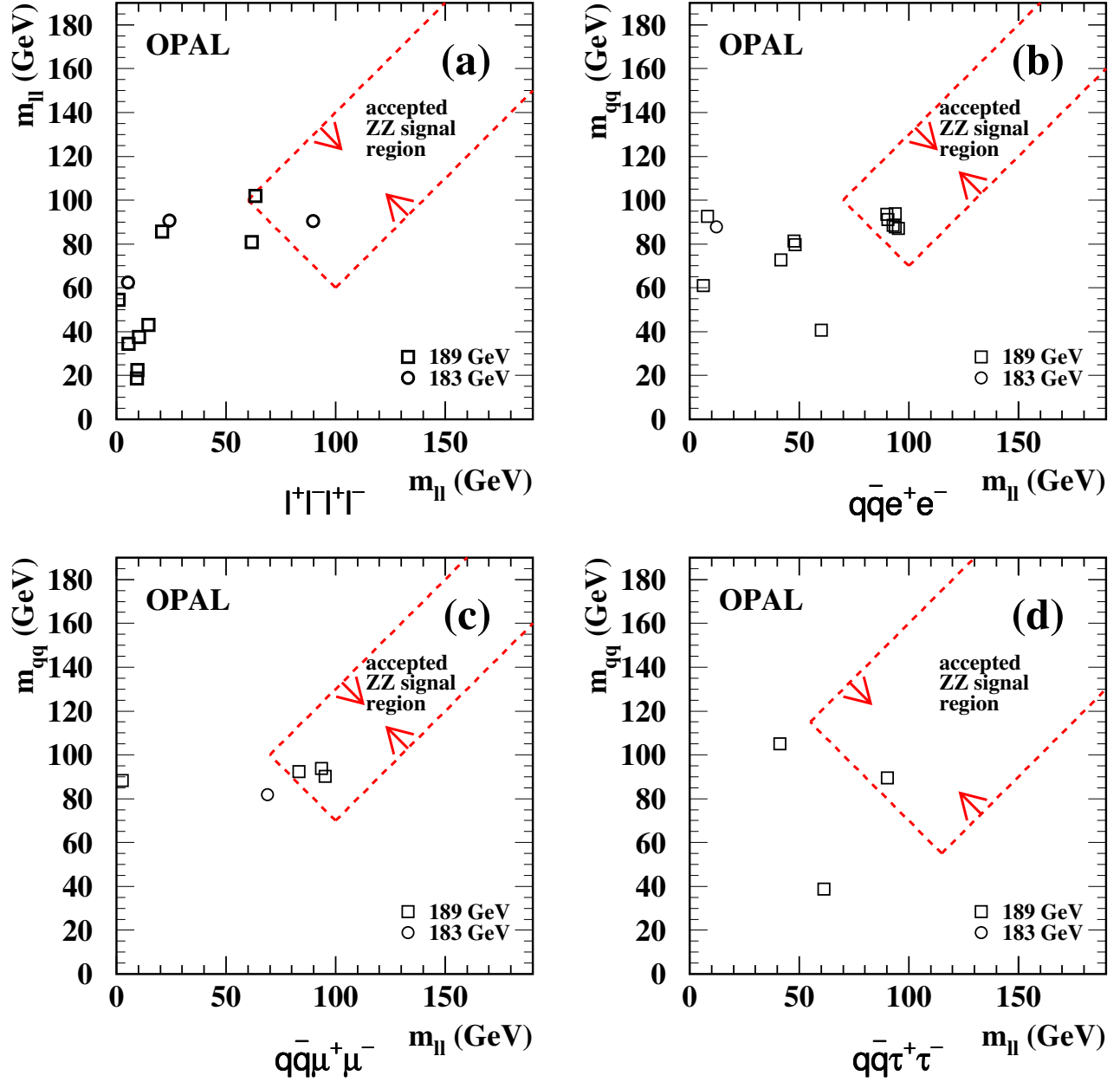


Figure 2: (a) Invariant masses of $\ell^+\ell^-\ell^+\ell^-$ cone pairs for the data at $\sqrt{s} = 183$ GeV and $\sqrt{s} = 189$ GeV. Invariant mass pairs for the (b) $q\bar{q}e^+e^-$ (c) $q\bar{q}\mu^+\mu^-$ and (d) $q\bar{q}\tau^+\tau^-$ data. The dashed lines show the final invariant mass cuts.

OPAL 189 GeV

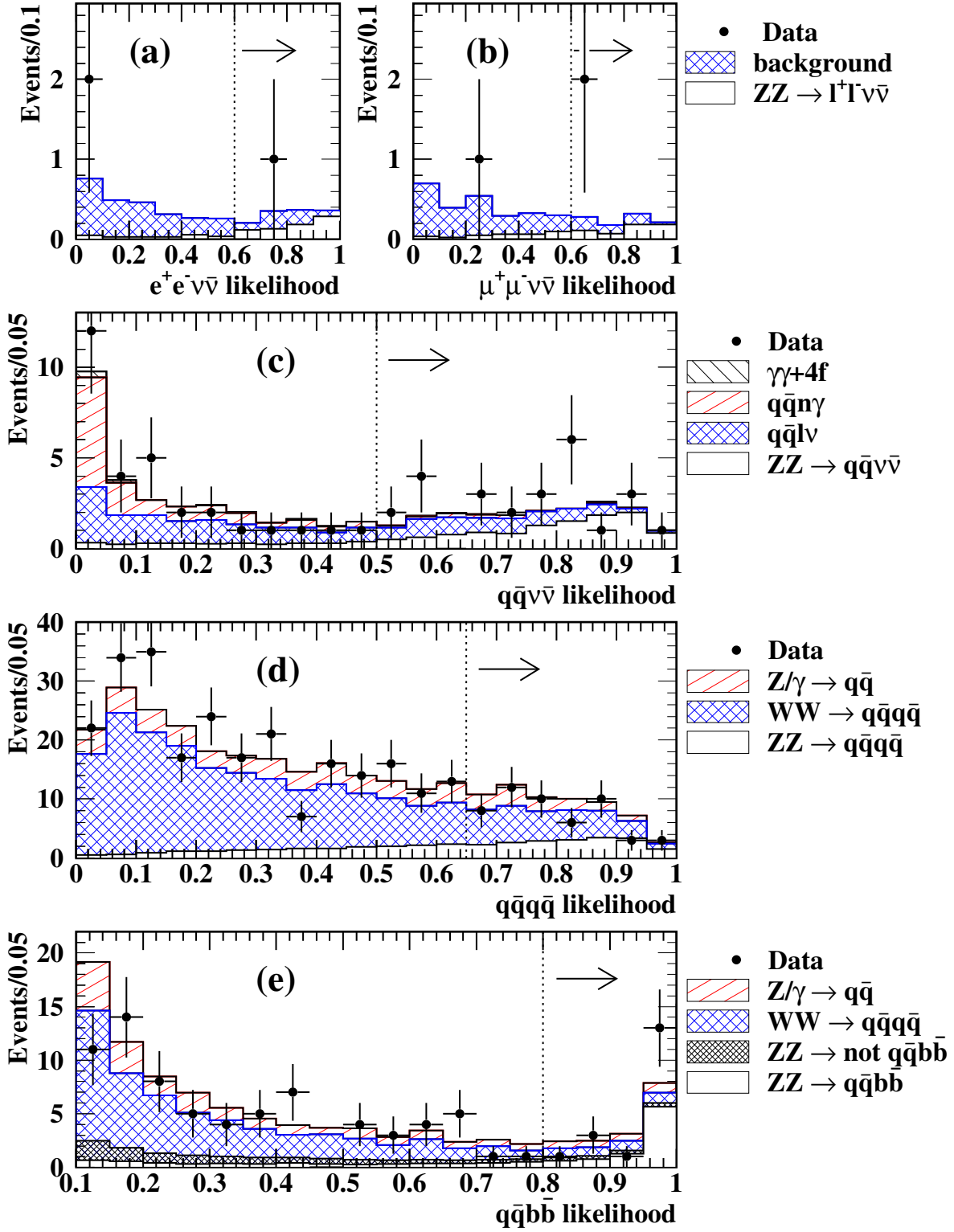


Figure 3: Likelihood discriminant used at $\sqrt{s} = 189$ GeV for (a) the $e^+e^- \nu\bar{\nu}$ selection, (b) the $\mu^+\mu^- \nu\bar{\nu}$ selection, (c) the $q\bar{q}\nu\bar{\nu}$ selection, (d) the $q\bar{q}q\bar{q}$ selection and (e) the $q\bar{q}b\bar{b}$ selection.

clusters, the rest of the event is forced into two jets. The 4C and 5C fits to the two lepton candidates and the two jets are required to converge.³

In the $q\bar{q}e^+e^-$ selection no explicit electron identification is used. Electron candidates are selected by requiring the sum of the electromagnetic cluster energies $E_1 + E_2$ associated to the electrons to be greater than 70 GeV and the momentum of the most energetic electron track to exceed 20 GeV. We also reject the event if the angle between either electron candidate and any other track is less than 5° .

In the $q\bar{q}\mu^+\mu^-$ selection the muons are identified using (i) tracks which match a reconstructed segment in the muon chambers, (ii) tracks which are associated to hits in the hadron calorimeter or muon chambers [27], or (iii) isolated tracks associated to electromagnetic clusters with reconstructed energy less than 2 GeV. No isolation requirement is imposed on events with both muon tracks passing (i) or (ii). Events with at least one muon identified with criterion (iii) are accepted if both muon candidates in the event have an angle of at least 10° to the nearest track. We require the sum of the momenta of the two leptons to be greater than 70 GeV.

Z-pair events are separated from $Z\gamma^*$ background by requiring the fitted mass of the 5C fit to be larger than 85 GeV and the invariant masses $m_{\ell\ell}$ and $m_{q\bar{q}}$ obtained from the 4C fit to satisfy $(m_{\ell\ell} + m_{q\bar{q}}) > 170$ GeV and $|m_{\ell\ell} - m_{q\bar{q}}| < 30$ GeV. Figure 2b (2c) shows the distribution of m_{ee} ($m_{\mu\mu}$) and $m_{q\bar{q}}$ before the cuts on the masses from the 4C and 5C fits.

After all cuts the selection efficiency⁴ for $q\bar{q}e^+e^-$ signal events is $(55.2 \pm 2.7)\%$ at 183 GeV and $(65.1 \pm 2.9)\%$ at 189 GeV. The errors on these efficiencies include the systematic errors (see Section 3.6). No candidate is observed at 183 GeV. Six candidate events are found after all cuts in the data taken at 189 GeV. In Table 1 (lines d and e) we give the efficiency, background and observed number of events. The largest source of background after all cuts is from $Z\gamma^*$ mediated $q\bar{q}e^+e^-$ events and from two-photon events.

For the $q\bar{q}\mu^+\mu^-$ final state the selection efficiency is $(66.9 \pm 2.6)\%$ at 183 GeV and $(72.3 \pm 2.8)\%$ at 189 GeV. Three events are observed in the 189 GeV data sample and none in the 183 GeV data sample. The errors on these efficiencies include the systematic errors given below. In Table 1 (lines f and g) we give the efficiency, backgrounds and observed number of events. The background after all cuts is expected to come from $e^+e^- \rightarrow Z\gamma^* \rightarrow q\bar{q}\mu^+\mu^-$ events.

3.3.2 Selection of $e^+e^- \rightarrow ZZ \rightarrow q\bar{q}\tau^+\tau^-$ events

The $q\bar{q}\tau^+\tau^-$ final state is selected from a sample of events with track multiplicity greater or equal to six. Events which have been selected as $e^+e^- \rightarrow ZZ \rightarrow q\bar{q}e^+e^-$ or $e^+e^- \rightarrow ZZ \rightarrow q\bar{q}\mu^+\mu^-$ are excluded from this selection. The tau-lepton candidates are selected using an artificial neural network algorithm which is described in detail in Reference [6]. The tau candidate with the highest neural network output value is taken as the first candidate. The second best candidate is required to have its charge opposite to the first candidate and the highest output value among all remaining candidates. If a second candidate cannot be found the event is rejected.

Motivated by the presence of neutrinos in the final state, the visible energy of the event, E_{vis} , is required to exceed 90 GeV and the missing energy $\sqrt{s} - E_{\text{vis}}$ is required to exceed 15 GeV. In addition, the sum of the momenta of the leading tracks from the tau-lepton decays is required to be less than 70 GeV. Since the direction of the missing momentum in signal events will tend to be along the direction of one of the decaying tau leptons, the angle $\alpha_{\tau,\text{miss}}$ between the missing momentum and a tau-lepton candidate is required to satisfy $\alpha_{\tau,\text{miss}} < 90^\circ$ for at least one of the two tau candidates.

³ In the context of this paper, convergence is defined as a fit probability greater than 10^{-10} .

⁴ Small amounts of feedthrough from other ZZ final states, in this case $q\bar{q}\tau^+\tau^-$, are counted as signal.

The two hadronic jets are selected in the same way as in the $e^+e^- \rightarrow ZZ \rightarrow q\bar{q}e^+e^-$ selection. The initial estimate of the energy and the momenta of the tau candidates is found from the sum of the tracks associated to the tau by the neural network algorithm and all unassociated electromagnetic clusters in a cone with a half angle of 10° around the leading track from the tau decay. A 2C kinematic fit that imposes energy and momentum conservation (see the introduction to Section 3) is required to converge. A 3C kinematic fit, with the additional constraint of the equality of the fermion pair masses is also required to converge.

Using the network output [6] for each tau lepton, a probability is calculated taking into account the different branching ratios, sensitivities, efficiencies and background levels for 1-prong and 3-prong tau-lepton decays. In the following, we combine the probabilities \mathcal{P}_1 and \mathcal{P}_2 to form a likelihood using

$$\mathcal{L} = \frac{\mathcal{P}_1\mathcal{P}_2}{\mathcal{P}_1\mathcal{P}_2 + (1 - \mathcal{P}_1)(1 - \mathcal{P}_2)}. \quad (1)$$

The likelihood associated with probabilities of the two tau candidates is required to satisfy $\mathcal{L}_{\tau\tau} > 0.977$. In addition, the common mass of the 3C fit is required to exceed 85 GeV. Using the 2C fit masses of the tau pair, $m_{\tau\tau}$, and the quark pair, $m_{q\bar{q}}$, as obtained from the kinematic fit, we also require $m_{q\bar{q}} + m_{\tau\tau} > 170$ GeV and $|m_{q\bar{q}} - m_{\tau\tau}| < 60$ GeV.

After all cuts the selection efficiency for signal events is found to be $(22.2 \pm 1.7)\%$ at 183 GeV and $(26.9 \pm 2.0)\%$ at 189 GeV. One candidate event is found in the data at 189 GeV while no candidate is selected at 183 GeV. Figure 2d shows the masses of the candidate events before the invariant mass cuts. In Table 1 (lines h and i) we give the efficiencies, backgrounds and observed number of events.

3.3.3 Selection of $e^+e^- \rightarrow ZZ \rightarrow b\bar{b}\ell^+\ell^-$

Events with $b\bar{b}$ final states are selected using the algorithm described in Reference [6]. The b probabilities of the two hadronic jets are combined to form a likelihood, \mathcal{L}_{bb} , according to Equation 1. Because the $q\bar{q}e^+e^-$ and $q\bar{q}\mu^+\mu^-$ selections are pure, a relatively loose cut of $\mathcal{L}_{bb} > 0.2$ is used to select the $b\bar{b}e^+e^-$ and $b\bar{b}\mu^+\mu^-$ samples. For the selections with electron and muon pairs there are two classes of events since the selected $b\bar{b}\ell^+\ell^-$ events are a subset of the $q\bar{q}\ell^+\ell^-$ events. In Table 1 (lines e and g) we give the efficiencies of the b-tagged samples with respect to the expected fraction of $b\bar{b}$ events. The efficiencies for samples without b-tags are given with respect to the hadronic decays without $b\bar{b}$ final states.

In the $b\bar{b}e^+e^-$ selection one candidate is found in the data. The selection efficiency is found to be $(47 \pm 3)\%$ at 183 GeV and $(46 \pm 3)\%$ at 189 GeV.⁵ In the $b\bar{b}\mu^+\mu^-$ selection we find no candidate at 183 GeV and one candidate at 189 GeV. The selection efficiency is found to be $(50 \pm 3)\%$ at 183 GeV and $(54 \pm 3)\%$ at 189 GeV.

For the $b\bar{b}\tau^+\tau^-$ selection the $\mathcal{L}_{\tau\tau}$ cut of the $q\bar{q}\tau^+\tau^-$ selection is loosened and combined with \mathcal{L}_{bb} as follows. $\mathcal{L}_{\tau\tau}$ and \mathcal{L}_{bb} are both required to be greater than 0.1. The $b\bar{b}\tau^+\tau^-$ probability for the event, $\mathcal{L}_{bb\tau\tau}$, is calculated from Equation 1 with $\mathcal{L}_{\tau\tau}$ and \mathcal{L}_{bb} as inputs and required to exceed 0.95. After the cut on $\mathcal{L}_{bb\tau\tau}$, the remaining cuts of the $q\bar{q}\tau^+\tau^-$ selection are applied, giving a selection efficiency of $(21 \pm 3)\%$ at 183 GeV and $(24 \pm 3)\%$ at 189 GeV. No candidate event is found in the 183 GeV or 189 GeV data.

We also use an alternative jet-based $b\bar{b}\tau^+\tau^-$ selection [6] and accept any event which passes either $b\bar{b}\tau^+\tau^-$ analysis, but events previously selected by another $q\bar{q}\ell^+\ell^-$ selection are rejected. The alternative analysis uses a different approach to reconstruct the tau leptons. This event selection

⁵ The efficiencies given in this section do not include feedthrough from other $q\bar{q}\ell^+\ell^-$ final states. The efficiencies given in Table 1 include this feedthrough.

consists of a set of preselection cuts and a subsequent multivariate likelihood selection. Events are reconstructed as four jets using the Durham algorithm. Tau-lepton candidates are sought in the four jets using a likelihood technique to separate real tau leptons and fakes in quark jets. The tau and b-tag likelihood values are combined in a $b\bar{b}\tau^+\tau^-$ likelihood which is maximized to choose the b jets and tau leptons of the event. This $b\bar{b}\tau^+\tau^-$ likelihood uses tau and b-tag likelihoods and some topological variables as input. Events are accepted if their likelihood exceeds 0.6. In addition, the fitted 2C masses are required to satisfy $m_{q\bar{q}} + m_{\tau\tau} > 170$ GeV and $|m_{q\bar{q}} - m_{\tau\tau}| < 60$ GeV.

At 189 GeV data the alternative selection has an efficiency of $(30 \pm 3)\%$ for $b\bar{b}\tau^+\tau^-$ events. After combining the two selections, the efficiency for $b\bar{b}\tau^+\tau^-$ events for all cuts except those rejecting events found by the other $q\bar{q}\ell^+\ell^-$ selections is 40%. A similar improvement is realized for the 183 GeV data. The efficiency and backgrounds after rejecting events found by the other selections are given in Table 1 (line j). One exclusive event is selected by the combined $b\bar{b}\tau^+\tau^-$ analysis at 189 GeV.

3.4 Selection of $ZZ \rightarrow q\bar{q}\nu\bar{\nu}$ events

The $q\bar{q}\nu\bar{\nu}$ selection is based on the reconstruction of the Z boson decaying to $q\bar{q}$ which produces somewhat back-to-back jets. The selection uses contained events with a two-jet topology. The beam energy constraint is then used to determine the mass of the Z boson decaying to $\nu\bar{\nu}$. The properties of the $q\bar{q}$ decay and the inferred mass of the $\nu\bar{\nu}$ decay are then used in a likelihood analysis to separate signal from background.

Two-jet events are selected by dividing each event into two hemispheres using the plane perpendicular to the thrust axis. The number of charged tracks in each hemisphere is required to be four or more. The polar angles of the energy-momentum vector associated with each hemisphere, θ_{hemi1} and θ_{hemi2} , are used to calculate the quantity $\cos\theta_h = \frac{1}{2}(\cos\theta_{\text{hemi1}} - \cos\theta_{\text{hemi2}})$. Contained events are selected by requiring $|\cos\theta_h| < 0.80$. The total energy in the forward detectors and in the forward region of the electromagnetic calorimeter ($|\cos\theta| > 0.95$) is required to be less than 3 GeV. W decays identified by the OPAL W-pair selection are rejected; the likelihood for $e^+e^- \rightarrow q\bar{q}\ell\nu$ from Reference [27], \mathcal{L}_{WW} , is required to be 0.5 or less.

An important background to our selection is $q\bar{q}(n\gamma)$ events with photons which escape detection. We discriminate against these events by looking for a significant amount of missing transverse momentum, p_t . In each event, p_t can be resolved into two components, p_{ti} , perpendicular to both the thrust axis and the beam axis and p_{tj} , along the thrust axis and perpendicular to the beam axis. Since p_{ti} is based primarily on angular measurements, it is better measured than p_{tj} . We approximate p_{ti} as $p_{ti} = \frac{1}{2}E_b \sin\phi \sin\theta_h$. Here $E_b = \sqrt{s}/2$ is the beam energy, ϕ is the acoplanarity of the momentum vectors of the two hemispheres and $\sin\theta_h = \sqrt{1 - \cos^2\theta_h}$. The resolution on p_{ti} , $\sigma_{p_{ti}}$, was parameterized as a function of thrust and $\cos\theta_h$ using data taken at the Z resonance. The variable $R_{p_{ti}} = (p_{ti} - p_{ti}^0)/\sigma_{p_{ti}}$ is used as an input to the likelihood. Here p_{ti}^0 corresponds to the transverse momentum carried by a photon with half the beam energy which just misses the inner edge of our acceptance ($p_{ti}^0 = E_b \sin(32 \text{ mrad})/2$). We also use the variable $\cos\theta_{\text{miss}}$, the direction of the missing momentum in the event, to discriminate against the $q\bar{q}(n\gamma)$ events.

In the final selection of events, we use a likelihood based on the following five variables: (i) the normalized sum of visible and recoil masses $(m_{\text{vis}} + m_{\text{recoil}})/\sqrt{s}$, (ii) the difference of visible and recoil masses $(m_{\text{vis}} - m_{\text{recoil}})$, (iii) $\log(y_{23})$, where y_{23} is the jet resolution parameter that separates the two-jet topology from the three-jet topology as calculated from the Durham jet algorithm, (iv) $\cos\theta_{\text{miss}}$ and (v) $R_{p_{ti}}$. The mass variables are useful for reducing background from W-pair production and $W\ell\nu$ final states. The jet resolution parameter is useful in reducing the remaining $q\bar{q}\ell\nu$ final states. To improve the performance of the likelihood analysis we use only events with: $|m_{\text{vis}} - m_{\text{recoil}}| < 50$ GeV, $(m_{\text{vis}} + m_{\text{recoil}})/\sqrt{s} > 0.89$ and $R_{p_{ti}} > 1.2$. Events are then selected using $\mathcal{L}_{q\bar{q}\nu\bar{\nu}} > 0.5$, where $\mathcal{L}_{q\bar{q}\nu\bar{\nu}}$

is the likelihood for the $q\bar{q}\nu\bar{\nu}$ selection. The likelihood distribution of data and Monte Carlo is shown in Figure 3c. For the $b\bar{b}\nu\bar{\nu}$ selection we require, in addition, the b-tag variable of Reference [6] to be greater than 0.65.

The efficiencies for the $q\bar{q}\nu\bar{\nu}$ selection alone are $(30.5 \pm 2.0)\%$ at 183 GeV and $(33.9 \pm 2.3)\%$ at 189 GeV. The errors on these efficiencies include the systematic errors discussed below in Section 3.6. The efficiencies after considering the results of the b-tagging, as well as the number of events selected at the two energies are given in Table 1 (lines k and l).

3.5 Selection of $ZZ \rightarrow q\bar{q}q\bar{q}$ events

The fully hadronic channel of the Z-pair decay has the largest branching fraction of all channels (about 50%), but suffers from large background from hadronic W-pair decays. We apply two different event selections, one of which is based mainly on reconstructed mass information in order to accept all hadronic Z-pair decays without flavor requirement, while a second analysis applies a flavor tag in order to select final states involving b quarks, allowing for looser requirements on the reconstructed boson mass.

For both subsamples, hadronic $Z^*/\gamma^* \rightarrow q\bar{q}$ events are an important background. We therefore start with a common preselection based on event shape variables which is mainly aimed at reducing this background. We use a likelihood method, described below in Section 3.5.1, in order to choose the most likely jet pairing for Z-pair decays.

3.5.1 Preselection and jet pairing

The event selection starts from the inclusive multihadron selection described in Reference [13]. The radiative process $e^+e^- \rightarrow Z\gamma \rightarrow q\bar{q}\gamma$ is suppressed by requiring the effective center-of-mass energy after initial state radiation, $\sqrt{s'}$, to be larger than 150 GeV. $\sqrt{s'}$ is obtained from a kinematic fit [13] that allows for one or more radiative photons in the detector or along the beam pipe. The final state particles are then grouped into jets using the Durham algorithm [28]. A four-jet sample is formed by requiring the jet resolution parameter y_{34} to be at least 0.003 and each jet to contain at least two charged tracks. In order to suppress $Z^*/\gamma^* \rightarrow q\bar{q}$ background, the event shape parameter C_{par} [30], which is large for spherical events, is required to be greater than 0.25. A 4C kinematic fit using energy and momentum conservation is required to converge. A 5C kinematic fit which forces the two jet pairs to have the same mass is applied in turn to all three possible combinations of the four jets. This fit is required to converge for at least one combination. The efficiencies of these preselection cuts are $(86.4 \pm 0.5)\%$ and $(88.9 \pm 0.5)\%$ for signal events at 183 GeV and 189 GeV, respectively.

In order to determine which pair of jets comes from each Z, we calculate a likelihood function using the mass obtained from the 5C fit, the corresponding fit probability, and the difference between the two di-jet masses obtained from the 4C fit. In the YFSZZ simulation of Z-pair decays the correct jet pairing has the highest likelihood output in $(86.8 \pm 0.5)\%$ of the events. This fraction rises to $(93.8 \pm 0.5)\%$ for the events after the final selection.

3.5.2 Likelihood for the inclusive $ZZ \rightarrow q\bar{q}q\bar{q}$ event selection

We use a likelihood selection with eight input variables for the selection of $ZZ \rightarrow q\bar{q}q\bar{q}$ events. The first variable is the jet pairing likelihood described above. Excluding the jet pairing with the largest difference between the two di-jet masses as obtained from the 4C fit, we identify among the remaining two possible pairings the one for which the 5C-fit mass is closer to the W mass. We use the difference between this 5C-fit mass and the W mass in order to discriminate against hadronic W-pair events.

Two variables that are sensitive to unobserved particles along the beam direction are the fitted center-of-mass energy and the sum of the cosines of the polar angles of the four jets. In order to discriminate against Z^*/γ^* events, we use the difference between the largest and smallest jet energies after the 4C fit, and the angular variable $j_{\text{ang}} = E_4(1 - \cos \theta_{12} \cos \theta_{13} \cos \theta_{23})/\sqrt{s}$, where E_4 is the smallest of the four jet energies, and the θ_{ij} are the opening angles between jets i and j , with the jets ordered by energy. Finally we calculate from the momenta configuration of the four jets the effective matrix element for the QCD processes $Z^*/\gamma^* \rightarrow q\bar{q}g$ and $Z^*/\gamma^* \rightarrow q\bar{q}q\bar{q}$ as defined in Reference [29], and the matrix element for the process $WW \rightarrow q\bar{q}q\bar{q}$ from Reference [23].

The distribution of the likelihood function calculated from these eight variables is shown in Figure 3d. In order to maximize the significance of the measured cross section, assuming a 10% relative systematic error on the background, we place a cut on the likelihood at 0.65. This cut leads to an efficiency of $(33.0 \pm 1.8)\%$ (189 GeV) relative to all fully hadronic NC2 Z-pair final states. In the data, 52 events are selected. We expect a total of 57.0 events from Standard Model processes, of which 17.6 originate from the Z-pair signal, while 27.0 events are expected from hadronic W-pair decays and 12.4 events from hadronic two-fermion processes. At 183 GeV the selection efficiency for fully hadronic Z-pair decays is $(25.3 \pm 1.3)\%$. In the data 8 events are selected. The Standard Model expectation is 1.7 signal events and 7.2 background events.

3.5.3 Likelihood for $ZZ \rightarrow q\bar{q}b\bar{b}$ event selection

Jets originating from b-quarks are selected using the same b-tagging algorithm used in the $b\bar{b}\ell^+\ell^-$ and $b\bar{b}\nu\bar{\nu}$ selections. We evaluate the probability for each of the four jets to originate from a primary b quark, and use the two highest probabilities as input variables for a likelihood to select $ZZ \rightarrow q\bar{q}b\bar{b}$ events. In addition, we use the parameters y_{34} , C_{par} , the difference between the largest and smallest jet energies and the output of the jet pairing likelihood. We also use the fit probabilities of a 5C kinematic fit which constrains one boson mass to the Z mass, and the probability of a 6C fit which forces both masses to be equal to the W mass.

Figure 3e shows the distribution of the likelihood function calculated from these eight variables for the preselected events. The signal likelihood is required to be larger than 0.80 for both 183 GeV and 189 GeV data. After the likelihood selection, we perform an additional cut on the mass obtained from the 5C-mass fit in the most likely jet pairing, which is required to be larger than 86 GeV. This choice of the cuts on the likelihood and on the 5C-fit mass was made by maximizing the expected statistical significance of signal over background. The final efficiency is $(35.1 \pm 2.4)\%$ for the 183 GeV data and $(38.6 \pm 2.7)\%$ for the 189 GeV data. The observed number of events, expected signal and background are given in Table 1 (line o).

3.5.4 Combination

To account for overlap between the $q\bar{q}q\bar{q}$ and $q\bar{q}b\bar{b}$ selections we divide the data into three logical classes, exclusive $q\bar{q}q\bar{q}$ events (Table 1 (line m)), exclusive $q\bar{q}b\bar{b}$ (line n) events and the overlapping region (Table 1 (line o)). In Table 1 (line m) we give the efficiency relative to all fully hadronic final states without b-quarks. The other efficiencies are given relative to fully hadronic final states with b-quarks.

3.6 Selection systematic errors

Systematic errors have only a modest effect on our final result because of the large statistical error associated with the small Z-pair cross section.

Detector effects can best be studied by comparing calibration data taken at the Z resonance with a simulation of the same process. These comparisons are important for final states such as $\ell^+\ell^-\nu\bar{\nu}$, $q\bar{q}\nu\bar{\nu}$, and $q\bar{q}q\bar{q}$, where the tight cuts are needed to separate signal and background. In these cases, we add additional smearing to the energy and momentum of the simulated events to match data and simulation. We then apply the same smearing to the signal and background Monte Carlos and then correct our efficiencies and background accordingly. The full difference is used as the systematic error in these cases. At $\sqrt{s} = 189$ GeV, these differences give relative systematic errors on the efficiency of 2.5% for the $e^+e^-\nu\bar{\nu}$ final state, 5.2% for the $\mu^+\mu^-\nu\bar{\nu}$ final state and 3.8% for $q\bar{q}\nu\bar{\nu}$ final state. In the $q\bar{q}q\bar{q}$ inclusive analysis, where uncertainties on the reconstructed angles are also important, similar studies lead to a relative detector systematic error of 6%.

Detector systematic errors for the $q\bar{q}\ell^+\ell^-$ and $\ell^+\ell^-\ell^+\ell^-$ selections without τ -pairs in the final state are small because of the good separation of signal and background. In the $\ell^+\ell^-\ell^+\ell^-$ final state the largest effect (3%) is from modeling of the multiplicity requirement which is important for final states containing τ -pairs. In the $q\bar{q}\tau^+\tau^-$ selection, the systematic uncertainties in the efficiencies were determined by overlaying hadronic and tau decays taken from Z resonance data giving a contribution to the systematic error of 6.0%. When the final states are combined to determine the cross section and limits on the anomalous triple gauge couplings, we assume a common relative systematic error of 3% on the efficiencies.

Another important detector effect comes from the simulation of the variables used by the OPAL b-tag which is discussed in Reference [6]. We allow for a common 5% error in the efficiency of the b-tag, consistent with our studies on Z resonance data and Monte Carlo.

These detector effects were propagated through to our background errors.

In each channel the signal and background Monte Carlo generators have been compared against alternative generators. In almost all cases the observed differences are consistent within the finite Monte Carlo statistics and the systematic error has been assigned accordingly. One notable exception is in the $q\bar{q}b\bar{b}$ background where differences in the PYTHIA, grc4f and EXCALIBUR simulation of the W-pair background are as large as 20%. In this case the full difference has been assigned as the systematic error.

In the $\ell^+\ell^-\ell^+\ell^-$ channels, which has a large background from two-photon events, we have compared the number of selected events at an early stage of the analysis with the Monte Carlo prediction and based our background systematic error on the level of agreement. This results in 20% systematic error.

4 Results

We combine the information from all of the analyses reported above using a maximum likelihood fit to determine the production cross section for $e^+e^- \rightarrow ZZ$. The information which was used in the fit, as well as the Standard Model prediction for Z-pair production, is summarized in Table 1. For each channel the table gives the number of events observed, n_{obs} , the Standard Model prediction for all events, n_{SM} , the expected signal, n_{ZZ} , the expected background, n_{back} , the efficiency ϵ_{chan} , and the integrated luminosity, L_{int} . B_{ZZ} is the branching ratio of Z-pairs to the given final state, calculated from Z resonance data [2]. In the table we give the overlap between the b-tag and non-b-tag analyses. Possible overlap between $q\bar{q}q\bar{q}$ and $q\bar{q}\ell^+\ell^-$ has been studied, and found to be an order of magnitude smaller than the overlap of $q\bar{q}q\bar{q}$ and $q\bar{q}b\bar{b}$ and has therefore been ignored.

The cross section at each energy is determined with a maximum likelihood fit using a Poisson probability density convolved with Gaussians to describe the uncertainties on efficiencies and backgrounds. The expected number of events in each channel, μ_e , as function of the Z-pair cross section,

$$\sqrt{s} = 183 \text{ GeV}$$

	Selection	n_{obs}	n_{SM}	n_{ZZ}	n_{back}	ϵ_{chan}	B_{ZZ}	L_{int} (pb^{-1})
a	$\ell^+\ell^-\ell^+\ell^-$	1	0.15 ± 0.03	0.07 ± 0.01	0.08 ± 0.03	0.54 ± 0.02	0.010	56.7
b	$e^+e^-\nu\bar{\nu}$	0	0.15 ± 0.04	0.06 ± 0.01	0.09 ± 0.03	0.34 ± 0.05	0.013	56.8
c	$\mu^+\mu^-\nu\bar{\nu}$	0	0.06 ± 0.02	0.04 ± 0.01	0.03 ± 0.02	0.20 ± 0.03	0.013	56.8
d	$q\bar{q}e^+e^- \& \overline{b\bar{b}e^+e^-}$	0	0.41 ± 0.04	0.27 ± 0.01	0.14 ± 0.04	0.56 ± 0.03	0.037	54.7
e	$q\bar{q}e^+e^- \& \overline{b\bar{b}e^+e^-}$	0	0.10 ± 0.02	0.07 ± 0.01	0.03 ± 0.02	0.52 ± 0.05	0.010	54.7
f	$q\bar{q}\mu^+\mu^- \& \overline{b\bar{b}\mu^+\mu^-}$	0	0.40 ± 0.03	0.34 ± 0.01	0.07 ± 0.03	0.70 ± 0.02	0.037	54.7
g	$q\bar{q}\mu^+\mu^- \& \overline{b\bar{b}\mu^+\mu^-}$	0	0.08 ± 0.01	0.08 ± 0.01	0.01 ± 0.01	0.57 ± 0.05	0.010	54.7
h	$q\bar{q}\tau^+\tau^- \& \overline{b\bar{b}\tau^+\tau^-}$	0	0.20 ± 0.03	0.11 ± 0.01	0.09 ± 0.03	0.23 ± 0.02	0.037	54.7
i	$q\bar{q}\tau^+\tau^- \& \overline{b\bar{b}\tau^+\tau^-}$	0	0.03 ± 0.01	0.03 ± 0.01	0.00 ± 0.01	0.19 ± 0.03	0.010	54.7
j	$\overline{b\bar{b}\tau^+\tau^-} \& \overline{q\bar{q}\tau^+\tau^-}$	0	0.02 ± 0.01	0.02 ± 0.01	0.00 ± 0.01	0.13 ± 0.03	0.010	54.7
k	$q\bar{q}\nu\bar{\nu} \& \overline{b\bar{b}\nu\bar{\nu}}$	2	2.62 ± 0.25	0.87 ± 0.07	1.75 ± 0.24	0.30 ± 0.02	0.219	54.5
l	$q\bar{q}\nu\bar{\nu} \& \overline{b\bar{b}\nu\bar{\nu}}$	1	0.42 ± 0.06	0.25 ± 0.02	0.17 ± 0.06	0.31 ± 0.03	0.061	54.5
m	$q\bar{q}q\bar{q} \& \overline{q\bar{q}b\bar{b}}$	8	7.43 ± 0.70	1.03 ± 0.07	6.39 ± 0.69	0.26 ± 0.02	0.300	54.7
n	$q\bar{q}b\bar{b} \& \overline{q\bar{q}q\bar{q}}$	3	1.88 ± 0.31	0.47 ± 0.02	1.42 ± 0.31	0.15 ± 0.01	0.235	54.7
o	$q\bar{q}b\bar{b} \& \overline{q\bar{q}q\bar{q}}$	0	1.41 ± 0.19	0.61 ± 0.03	0.80 ± 0.19	0.20 ± 0.01	0.235	54.7

$$\sqrt{s} = 189 \text{ GeV}$$

	Selection	n_{obs}	n_{SM}	n_{ZZ}	n_{back}	ϵ_{chan}	B_{ZZ}	L_{int} (pb^{-1})
a	$\ell^+\ell^-\ell^+\ell^-$	1	1.02 ± 0.21	0.68 ± 0.02	0.35 ± 0.21	0.58 ± 0.02	0.010	182.1
b	$e^+e^-\nu\bar{\nu}$	1	1.30 ± 0.17	0.72 ± 0.09	0.58 ± 0.15	0.46 ± 0.06	0.013	181.5
c	$\mu^+\mu^-\nu\bar{\nu}$	2	0.97 ± 0.15	0.54 ± 0.08	0.44 ± 0.13	0.35 ± 0.05	0.013	181.5
d	$q\bar{q}e^+e^- \& \overline{b\bar{b}e^+e^-}$	5	3.51 ± 0.38	2.79 ± 0.13	0.72 ± 0.36	0.69 ± 0.03	0.037	174.7
e	$q\bar{q}e^+e^- \& \overline{b\bar{b}e^+e^-}$	1	0.68 ± 0.07	0.59 ± 0.05	0.09 ± 0.06	0.52 ± 0.05	0.010	174.7
f	$q\bar{q}\mu^+\mu^- \& \overline{b\bar{b}\mu^+\mu^-}$	2	3.22 ± 0.12	3.05 ± 0.10	0.18 ± 0.08	0.75 ± 0.02	0.037	174.7
g	$q\bar{q}\mu^+\mu^- \& \overline{b\bar{b}\mu^+\mu^-}$	1	0.73 ± 0.04	0.71 ± 0.04	0.02 ± 0.02	0.63 ± 0.05	0.010	174.7
h	$q\bar{q}\tau^+\tau^- \& \overline{b\bar{b}\tau^+\tau^-}$	1	1.33 ± 0.13	1.14 ± 0.10	0.18 ± 0.08	0.28 ± 0.03	0.037	174.7
i	$q\bar{q}\tau^+\tau^- \& \overline{b\bar{b}\tau^+\tau^-}$	0	0.30 ± 0.06	0.25 ± 0.04	0.04 ± 0.04	0.22 ± 0.04	0.010	174.7
j	$\overline{b\bar{b}\tau^+\tau^-} \& \overline{q\bar{q}\tau^+\tau^-}$	1	0.29 ± 0.05	0.27 ± 0.04	0.02 ± 0.01	0.24 ± 0.04	0.010	174.7
k	$q\bar{q}\nu\bar{\nu} \& \overline{b\bar{b}\nu\bar{\nu}}$	20	16.1 ± 1.2	8.5 ± 0.7	7.51 ± 0.94	0.35 ± 0.03	0.219	174.2
l	$q\bar{q}\nu\bar{\nu} \& \overline{b\bar{b}\nu\bar{\nu}}$	5	2.18 ± 0.24	1.90 ± 0.20	0.28 ± 0.14	0.29 ± 0.03	0.061	174.2
m	$q\bar{q}q\bar{q} \& \overline{q\bar{q}b\bar{b}}$	45	50.1 ± 4.0	12.5 ± 0.8	37.6 ± 3.9	0.38 ± 0.03	0.300	174.7
n	$q\bar{q}b\bar{b} \& \overline{q\bar{q}q\bar{q}}$	11	6.74 ± 0.75	3.57 ± 0.23	3.16 ± 0.72	0.14 ± 0.01	0.235	174.7
o	$q\bar{q}b\bar{b} \& \overline{q\bar{q}q\bar{q}}$	7	7.87 ± 0.64	5.49 ± 0.32	2.38 ± 0.56	0.21 ± 0.02	0.235	174.7

Table 1: Observed number of events, n_{obs} , the total Standard Model expectation, n_{SM} , the expected number of Z-pairs, n_{ZZ} , background expectation, n_{back} , and efficiencies, ϵ_{chan} , for the 183 GeV and 189 GeV data. B_{ZZ} is the product branching ratio for the final state which is calculated directly from Z resonance data [2]. Note that the efficiencies for selections with b-tags are given relative to the fraction of hadronic final states which contain a Z boson decaying to $b\bar{b}$. For selections of events with hadronic final states, but without b-tags, the efficiencies are relative to those hadronic final states which do not include a Z boson decaying to $b\bar{b}$. The errors include contributions from the common systematic errors.

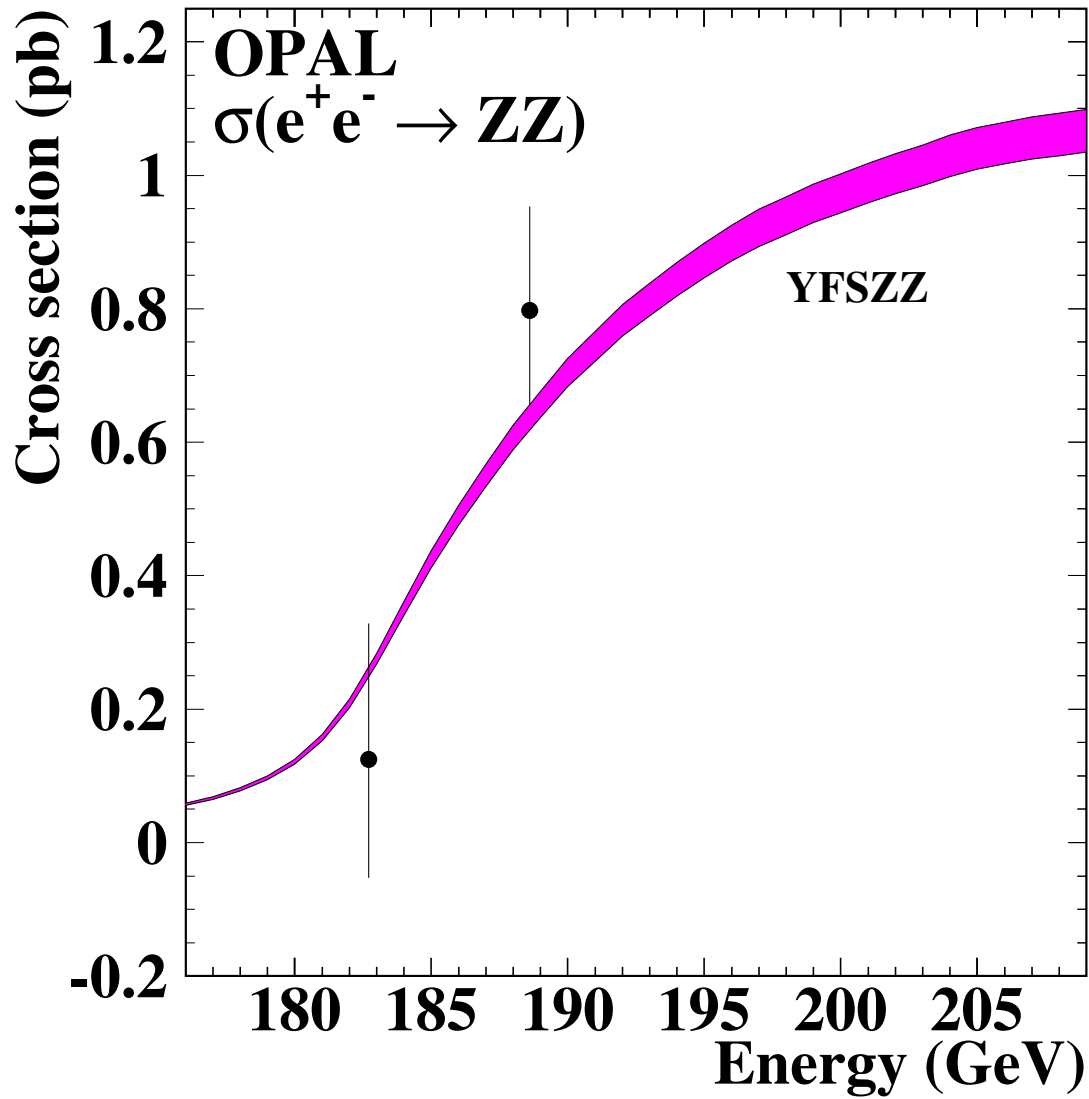


Figure 4: The OPAL measurements of the NC2 Z-pair production cross section. The shaded band shows the prediction, using the default settings, of the YFSZZ Monte Carlo for the total cross section. The band indicates a theoretical scale uncertainty of $\pm 3\%$.

σ_{ZZ} , is given by

$$\mu_e = \sigma_{ZZ} L_{\text{int}} \epsilon_{\text{chan}} B_{ZZ} + n_{\text{back}}. \quad (2)$$

The efficiencies, ϵ_{chan} , include the effects of off-shell Z bosons that are produced outside of our kinematic acceptance. Our main result, the NC2 Z-pair cross sections obtained from the fits, is

$$\begin{aligned} \sigma_{ZZ}(183 \text{ GeV}) &= 0.12^{+0.20}_{-0.18}(\text{stat.})^{+0.03}_{-0.02}(\text{syst.}) \text{ pb} \\ \sigma_{ZZ}(189 \text{ GeV}) &= 0.80^{+0.14}_{-0.13}(\text{stat.})^{+0.06}_{-0.05}(\text{syst.}) \text{ pb}. \end{aligned}$$

The 183 GeV result corresponds to a 95% C.L. upper limit (normalized to the region $\sigma_{ZZ} > 0$) of 0.55 pb. The comparison of these measurements with the YFSZZ prediction, using the coupling of Z bosons to electrons measured at the Z resonance, is shown in Figure 4. The results are consistent with the YFSZZ prediction and with the measurements presented in Reference [31].

Our results assume that, apart from the backgrounds discussed above, only ZZ production contributes inside our kinematic region. Possible effects of Higgs boson production have been ignored.

In order to check the results for consistency with the expected fraction of $b\bar{b}$ final states, we perform a second fit where the branching ratio of the Z boson to $b\bar{b}$ is a free parameter. The relative branching ratios of the Z to other fermion pairs are fixed to their measured values. The resulting branching ratio and cross section for the 189 GeV data are $\text{Br}(Z \rightarrow b\bar{b}) = 0.21^{+0.07}_{-0.06}(\text{stat.}) \pm 0.01(\text{syst.})$ and $\sigma_{ZZ} = 0.75^{+0.15}_{-0.14}(\text{stat.})^{+0.06}_{-0.05}(\text{syst.})\text{pb}$. The measured branching ratio can be compared with the world average as measured at the Z resonance of $\text{Br}(Z \rightarrow b\bar{b}) = 0.1516 \pm 0.0009$ [2]. The cross section measured without constraining the branching ratio is also consistent with our main result and the YFSZZ prediction. The smaller error on the main result cross section illustrates the advantage of classifying the hadronic systems as $b\bar{b}$ or non- $b\bar{b}$. The 183 GeV data sample is too small to extract a meaningful value of the $Z \rightarrow b\bar{b}$ branching ratio.

Limits on anomalous triple gauge couplings were set using the total cross section and the $|\cos \theta_Z|$ distribution of our data. Here θ_Z is the polar angle of the Z bosons produced. In this study we varied the real and imaginary parts of the ZZZ and ZZ γ anomalous couplings parameterized by the form factors f_4^{ZZZ} , f_5^{ZZZ} , $f_4^{ZZ\gamma}$ and $f_5^{ZZ\gamma}$ as defined in Reference [3] and implemented in the YFSZZ Monte Carlo. The real and imaginary parts of each coupling were varied separately with all others fixed to zero.

For this study we consider the effect of the anomalous couplings on the total cross section at $\sqrt{s} = 183 \text{ GeV}$ and on the cross section in four bins of $|\cos \theta_Z|$ at $\sqrt{s} = 189 \text{ GeV}$. The selection efficiencies for all final states are parameterized as function of anomalous couplings. At $\sqrt{s} = 189 \text{ GeV}$ the parameterization is done separately for each bin in $|\cos \theta_Z|$. For values of the anomalous couplings larger than unity, much of the production of the final state fermions occurs at $|\cos \theta| \simeq 1$ where the efficiency for most channels is reduced by a factor of ~ 0.5 . An uncertainty of 10%, dominated by Monte Carlo statistical errors, is assigned to the correction we apply to these efficiencies.

The 95% C.L. limits on the anomalous couplings obtained from the maximum likelihood fit are given in Table 2. With the exception of the $\text{Re}\{f_5^{ZZZ}\}$ coupling, the limits are insensitive to the sign and complex phase of the couplings.

5 Conclusion

The production cross section of $e^+e^- \rightarrow ZZ$ has been measured using the final states $\ell^+\ell^-\ell^+\ell^-$, $\ell^+\ell^-\nu\bar{\nu}$, $q\bar{q}\ell^+\ell^-$, $q\bar{q}\nu\bar{\nu}$, and $q\bar{q}q\bar{q}$. The number of observed events, the background expectation from Monte Carlo and the calculated efficiencies have been combined to measure the production cross

Coupling	95% C.L. Lower Limit	95% C.L. Upper Limit
$Re\{f_4^{ZZZ}\}$	-2.1	2.1
$Im\{f_4^{ZZZ}\}$	-2.1	2.1
$Re\{f_5^{ZZZ}\}$	-6.2	4.4
$Im\{f_5^{ZZZ}\}$	-6.4	6.4
$Re\{f_4^{ZZ\gamma}\}$	-1.2	1.2
$Im\{f_4^{ZZ\gamma}\}$	-1.2	1.2
$Re\{f_5^{ZZ\gamma}\}$	-3.9	3.6
$Im\{f_5^{ZZ\gamma}\}$	-3.8	3.9

Table 2: The 95% confidence level limits on possible anomalous triple gauge couplings.

section of the process $e^+e^- \rightarrow ZZ$. Our measured cross sections include the effects of background and efficiency uncertainties.

We have determined the cross section for $e^+e^- \rightarrow ZZ$ separately at average center-of-mass energies of 182.62 ± 0.05 GeV and 188.63 ± 0.04 GeV. The NC2 Z-pair cross sections were determined to be

$$\sigma_{ZZ}(183 \text{ GeV}) = 0.12^{+0.20}_{-0.18}(\text{stat.})^{+0.03}_{-0.02}(\text{syst.}) \text{ pb}$$

$$\sigma_{ZZ}(189 \text{ GeV}) = 0.80^{+0.14}_{-0.13}(\text{stat.})^{+0.06}_{-0.05}(\text{syst.}) \text{ pb.}$$

At the lower center-of-mass energy, the 95% C.L. upper limit on the cross section is 0.55 pb. The measurements at both energies are consistent with the Standard Model expectations. No evidence is found for anomalous neutral current triple gauge couplings. The 95% confidence level limits are listed in Table 2.

Acknowledgements

We particularly wish to thank the SL Division for the efficient operation of the LEP accelerator at all energies and for their continuing close cooperation with our experimental group. We thank our colleagues from CEA, DAPNIA/SPP, CE-Saclay for their efforts over the years on the time-of-flight and trigger systems which we continue to use. In addition to the support staff at our own institutions we are pleased to acknowledge the

Department of Energy, USA,

National Science Foundation, USA,

Particle Physics and Astronomy Research Council, UK,

Natural Sciences and Engineering Research Council, Canada,

Israel Science Foundation, administered by the Israel Academy of Science and Humanities,

Minerva Gesellschaft,

Benozio Center for High Energy Physics,

Japanese Ministry of Education, Science and Culture (the Monbusho) and a grant under the Monbusho International Science Research Program,

Japanese Society for the Promotion of Science (JSPS),

German Israeli Bi-national Science Foundation (GIF),

Bundesministerium für Bildung, Wissenschaft, Forschung und Technologie, Germany,

National Research Council of Canada,

Research Corporation, USA,

Hungarian Foundation for Scientific Research, OTKA T-029328, T023793 and OTKA F-023259.

References

- [1] R.W. Brown and K.O. Mikaelian, Phys. Rev. **D19** (1979) 922.
- [2] C. Caso et al, Eur. Phys. J. **C3** (1998) 1.
- [3] K. Hagiwara, R.D. Peccei, D. Zeppenfeld and K. Hikasa, Nucl. Phys. **B282** (1987) 253.
- [4] D. Chang, W-Y Keung and P.B. Pal, Phys. Rev. **D51** (1995) 1326.
- [5] K. Agashe, N.G. Deshpande, Phys. Lett. **B456** (1999) 60.
- [6] OPAL Collab., G. Abbiendi et al., Eur. Phys. J. **C7** (1999) 407;
OPAL Collab., G. Abbiendi et al., *Search for Neutral Higgs Bosons in e^+e^- Collisions at $\sqrt{s}=189$ GeV*, CERN EP/99-096 Submitted to Eur. Phys. J. **C**.
- [7] OPAL Collab., K. Ahmet et al., Nucl. Instrum. Methods **A305** (1991) 275.
- [8] S. Anderson et al., Nucl. Instrum. Methods **A403** (1998) 326.
- [9] M. Arignon et al., Nucl. Instrum. Methods **313** (1992) 103;
M. Arignon et al., Nucl. Instrum. Methods **333** (1993) 330.
- [10] J.T. Baines et al., Nucl. Instrum. Methods **A325** (1993) 271;
D.G. Charlton, F. Meijers, T.J. Smith and P.S. Wells, Nucl. Instrum. Methods **A325** (1993) 129.
- [11] B.E. Anderson et al., IEEE Trans. Nucl. Sci. **41** (1994) 845;
OPAL Collab., G. Abbiendi et al., *Precision luminosity for Z lineshape measurements with a silicon-tungsten calorimeter*, CERN-EP/99-136, submitted to Eur. Phys. J. **C**.
- [12] LEP Energy Working Group, A. Blondel et al., *Evaluation of the LEP centre-of-mass energy above the W-pair production threshold*, CERN-EP/98-191, submitted to Eur. Phys. J. **C**;
Evaluation of the LEP centre-of-mass energy for data taken in 1998, LEP Energy Working Group, 99/01, March 1999.
- [13] OPAL Collab., K. Ackerstaff et al., Eur. Phys. J. **C2** (1998) 441.
- [14] OPAL Collab., K. Ackerstaff et al., Eur. Phys. J. **C6** (1999) 1.
- [15] S. Jadach et al., Comput. Phys. Commun. **102** (1997) 229;
S. Jadach, E. Richter-Wąs, B.F.L. Ward, Z. Wąs, Comput. Phys. Commun. **70** (1992) 305.
- [16] J. Allison et al., Nucl. Instrum. Methods **A317** (1992) 47.
- [17] J. Fujimoto et al., Comput. Phys. Commun. **100** (1997) 128.
- [18] S. Jadach, W. Placzek, B.F.L. Ward, Phys. Rev. **D56** (1997) 6939.
- [19] T. Sjöstrand, Comput. Phys. Commun. **82** (1994) 74.
- [20] G. Marchesini et al., Comput. Phys. Commun. **67** (1992) 465.
- [21] S. Jadach, B.F. Ward and Z. Wąs, Phys. Lett. **B449** (1999) 97.
- [22] S. Jadach, W. Placzek, M. Skrzypek, B.F. Ward and Z. Wąs, Comput. Phys. Commun. **119** (1999) 272.
- [23] F.A. Berends, R. Pittau, R. Kleiss, Comput. Phys. Commun. **85** (1995) 437.

- [24] A. Buijs et al., Comput. Phys. Commun. **79** (1994) 523.
- [25] J.A.M. Vermaseren, Nucl. Phys. **B229** (1983) 347.
- [26] OPAL Collab., G. Abbiendi et al., Phys. Lett. **B 438** (1998) 391.
- [27] OPAL Collab., K. Ackerstaff et al., Phys. Lett. **B389** (1996) 416;
OPAL Collab., K. Ackerstaff et al., Eur. Phys. J. **C1** (1998) 395;
OPAL Collab., G. Abbiendi et al., Eur. Phys. J. **C8** (1999) 191.
- [28] N. Brown and W. J. Stirling, Phys. Lett. **B252** (1990) 657;
S. Bethke, Z. Kunszt, D. Soper and W. J. Stirling, Nucl. Phys. **B370** (1992) 310;
S. Catani et al., Phys. Lett. **B269** (1991) 432;
N. Brown and W. J. Stirling, Z. Phys. **C53** (1992) 629.
- [29] S. Catani and M.H. Seymour, Phys. Lett. **B378** (1996) 287.
- [30] G. Parisi, Phys. Lett. **B74** (1978) 65;
J. F. Donoghue, F. E. Low and S. Y. Pi, Phys. Rev. **D20** (1979) 2759.
- [31] L3 Collab., M. Acciarri et al., Phys. Lett. **B450** (1999) 281;
L3 Collab., M. Acciarri et al., Phys. Lett. **B465** (1999) 363;
ALEPH Collab., R. Barate et al., CERN-EP/99-141, submitted to Phys. Lett. **B**.